Amino-Functionalised Zr-MOF Nanoparticles for Adsorption of CO_2 and CH_4

Hussein Rasool Abid[a], Jin Shang[b], Ha-Ming Ang[a], and Shaobin Wang[*a]

[a] Department of Chemical Engineering, Curtin University, GPO Box U1987, Perth, Western Australia 6845, Australia

[b] Department of Chemical Engineering, Monash University, Clayton, VIC 3800, Australia

Abstract

Amino functionalised Zr-MOF (amino-Zr-MOF) was synthesised using 2-aminoterephthalic acid as an organic linker. The physicochemical properties of the material were characterised by XRD, SEM, TGA, FTIR and N_2 adsorption to understand its crystalline structure, morphology, thermal stability, and porous structure. CO_2 adsorption isotherms on amino-Zr-MOF were obtained at 1 atm and different temperatures. In addition, CO_2 and CH_4 adsorption at high pressure (up to 10 atm) was also measured. CO_2 adsorption capacity on amino-Zr-MOF was 9 mmol/g at 988 kPa, 0 °C while CH_4 adsorption capacity was 3.7 mmol/g at 900 kPa and 0 °C. The heat of CO_2 adsorption on amino-Zr-MOF was estimated to be 29.4 kJ/mol. Continuous column tests of CO_2 adsorption were performed at different concentrations of CO_2 in nitrogen at 20 mL/min and 0.7 g adsorbent and total adsorbed amount of CO_2 within the column during the breakthrough time was calculated to be 4.55, 5.26 and 4.37 mmol/g at 10%, 15% and 20% CO_2, respectively.

Keywords: Zr-MOF, Amino-Zr-MOF, Carbon dioxide, Methane, Adsorption.

*Correspondence author. Email: Shaobin.Wang@curtin.edu.au

1. Introduction

Over the last few decades, carbon dioxide removal technologies from industrial emissions have been dependent on traditional methods, absorption and adsorption, which are very expensive and energy-intensive due to low capacity and selectivity of materials [1]. Metal organic frameworks (MOFs) as new emerging porous materials have been investigated to be alternative adsorbents for various industrial and environmental applications [2]. The applications of MOFs have covered several areas including gas purification and separation [3], gas storage [4], drug delivery [5] and catalysis, etc [6,7]. Unprecedentedly, MOFs have many characteristics such as ability to be designed with required specifications, high rigidity and flexibility to be functionalised, and exceptional low density [8]. The synthesis of MOFs can result in a robust extended framework with permanent porosity and these porosities may be fulfilled when the molecular building nets are connected by strong bonds [9, 10]. Previously, some transition metals have been used in the synthesis of MOFs, but priority is given to Zn and Al [2, 11].

Zirconium oxide (ZrO_2) has stable properties and the nature of zirconium atom connection with oxygen [12] makes it attractive in synthesis of MOFs. Moreover, it was observed that the synthesis of organic ligand of this framework could be controlled to get several Zr-MOFs (UiO-66, UiO-67 and UiO-68) [13]. Modification and application of Zr-MOFs have been also reported. Recently, Kandish et al. [14] synthesised Zr-MOF (UiO-66) with different functional groups by using different linker ligands, H_2N-H_2BDC, O_2N-H_2BDC, and Br-H_2BDC. Silva et al. [15] used both UiO-66 and UiO-66-NH_2 as photocatalysts for hydrogen generation while Vermoortele et al. [16] selected amino-UiO-66 for the cross-aldol condensation. These researchers used different procedures and molar ratios in the synthesis of amino-modified Zr-MOF. However, few investigations have been reported in Zr-MOF application for CH_4 and CO_2 adsorption [17].

In this work, we synthesised an amino-Zr-MOF sample by using a different precursor ratio and activation process at varying temperatures. The main work focused on the characteristics of this material and its application for CO_2 and CH_4 adsorption. Carbon dioxide adsorption capacity was determined at both low and high pressures while methane adsorption capacity was obtained at high pressure. Continuous column testes were also carried out for CO_2 adsorption.

2. Experimental

2.1 Chemicals

All chemicals including 2-amino-terephthalic acids (NH$_2$-BDC, 99%), terephthalic acid (BDC, 99.8%), zirconium chloride (ZrCl$_4$, 99.9%), dimethylformamide (DMF, 98%), methanol (CH$_3$OH, 99%) , chloroform (CHCl$_3$, 99.98%) were supplied by Sigma-Aldrich without further purification.

2.2 Synthesis and activation

Synthesis of Zr-MOF (UiO-66) follows a reported procedure [13]. In detail, 0.053 g of ZrCl$_4$ (0.227 mmol) and 0.034 g of 1,4-benzenedicarboxylic acid (H$_2$BDC, 0.227 mmol) were dissolved in 24.9 g of N,N-dimethylformamide (DMF, 340 mmol) at room temperature. The solution was placed in an autoclave of 45 mL and placed in a pre-heated oven at 120 ºC for 24 h. The final product was activated by immersing in chloroform for 4 d and then dried and heated under vacuum at 190 ºC overnight. This activation process was found to enhance the surface area and carbon dioxide adsorption [17].

In a typical procedure to synthesise amino-Zr-MOF (amino-UiO-66), 1.47 g (6.31 mmol) ZrCl$_4$ were dissolved in 15 mL DMF solution and stirring for around 20 min. Meanwhile, 1.06 g (5.85 mmol) NH$_2$-BDC were dissolved in 68 mL DMF solution and stirring for 30 min. Then, the two prepared solutions were mixed and placed in an autoclave of 125 mL. The sealed autoclave was then placed in an oven at 120 °C for 48 h. Finally, the greenish yellow crystalline product was extracted from the solution by vacuum filtration. The crystalline product was activated by immersing in methanol for 5 d, and then it was filtered, dried and heated under vacuum at 200 or 300 °C for 12 h. Methanol activation could remove the non-coordinated amino-BDC from the pores.

2.3 Characterisation of materials

A Perkin-Elmer 100 FT-IR spectrometer was used to investigate functional groups of crystalline materials. Scans were conducted from 650 to 4000 cm^{-1} with a resolution of 4 cm^{-1} using a universal ATR-Diamond/ZnSe as IR detector. Hydrothermal stability of the crystalline structure was checked by a TGA instrument (TGA/DSC1 STAR^e system-METTLER TOLEDO). A sample of 10 mg was loaded into an alumina pan and placed automatically in the TGA furnace to heat in Argon gas of 20 mL/min at a heating rate of 10 ºC/min from 35 to 900 ºC. X-ray powder diffraction patterns were measured on a X-ray diffractometer (D8 Advanced Bruker Axs) with a transmission mode using Cu *Kα* radiation at 2θ=5-70° to evaluate the stability of the crystalline structure. N$_2$ physisorption measurements were carried out on a Quantachrome instrument (Autosorb-1) at -196 °C. The surface area was obtained by the BET method and pore size distribution was determined by the BJH

method. In general, 15 mg of samples were degassed at 200 °C under vacuum for 6 h and then the sample was used in adsorption/desorption measurement on the same instrument. Morphology of materials including the shape and the size of crystals was determined by a SEM (Zeiss NEON 40 EsB CrossBeam) with high resolutions.

2.4 Adsorption at low pressure

A static volumetric technique with an apparatus of Micromeritics (Gemini I-2360) was used to determine adsorption isotherm of CO_2 (99.995%) at 0 and 23 °C, respectively, under pressure up to 100 kPa. In each test, about 0.3 g of amino-Zr-MOF was degassed by Vacprep 061 overnight at 200 °C under vacuum. The heat of CO_2 adsorption was calculated from the Clausius-Claperyron equation replying on the data of adsorption isotherms which were measured at different temperatures by the GemminiI-2360.

2.5 Adsorption at high pressure

A Micromeritics-ASAP2050 was used to measure the adsorption isotherms of carbon dioxide (99.995%) and methane (99.995%) at high pressure up to 1000 kPa. A sample was first degassed on the same instrument by increasing the temperature to 100 °C at a heating rate of 10 °C/min and hold at this temperature for 2 h. Then the temperature was increased again at the same heating rate to 200 °C under vacuum (up to 0.4 kPa) and hold at these conditions for 8 h. Finally, the degassed sample was used for the analysis at 0 °C.

2.6 Breakthrough experiments of CO_2 adsorption

CO_2 capture in a continuous column was tested by setting up breakthrough experiments. A mixture of N_2 (99.999%) and CO_2 (99.995%) in different molar concentrations (10, 15, and 20 mol% of CO_2) was used. A total flow rate at 20 mL/min during all breakthrough tests was maintained and controlled by calibrated mass flow controllers (GFC17-CO_2 and GFC-N_2, AALBORG). The stainless steel adsorption column has a length of 150 mm and inside diameter of 4 mm. In each run, 0.7 g of amino-Zr-MOF (particle size ranged from 0.1 to 1μm) was packed in the column with quartz wool on the ends of the column to avoid suspending of packed materials. A gas chromatograph instrument (GC-17A, Shimadzu) was used to measure the concentration of carbon dioxide effluent from the column by a TCD detector using He as a carriage gas.

3. Results and discussion

3.1 Characterisation of amino-Zr-MOFs

Fig.1 shows FTIR spectra of amino-Zr-MOF as-synthesised and activated by methanol and heating at varying temperatures. In Fig. 1a, the bands of 1400-1767 cm^{-1} are referred to carboxylic functional groups [18]. The carboxyl groups from free aromatic carboxylic acid were observed at 1656 cm^{-1} [19] on the as-synthesized sample; however, the peak was removed after heat activation, due to solvent extraction and heat treatment. For the samples of as-synthesized and activated at 200 °C, the band of 1430-1533 cm^{-1} was observed, indicating the presence of amino-carboxylate compounds that were coordinated with zirconium metal centre by –CO_2 asymmetrical stretching with the peaks at 1497 cm^{-1} and 1564 cm^{-1} or –CO_2 symmetrical stretching with the peaks at 1385 and 1424 cm^{-1} [18, 20, 21]. From magnification part of the spectrum of as-synthesized amino-Zr-MOF (Fig.1b), two peaks with much lower intensities appearing at 3376 and 3457 cm^{-1} were related to primary amines, -NH_2, on the organic linker. Low intensities of these peaks before heat activation may be attributed to the strong bonding between the amino groups on the coordinated acid with C=O groups of free NH_2-BDC inside the pores and bridging OH groups on the metal centre (bridging OH groups can interact with amino groups on the organic linker by hydrogen bond) [22, 23]. In addition, the amino group of organic linker was affected by moisture from the surroundings by hydrogen bonding interaction. After activation at 200 °C, a small shift in the position of amino-groups stretching can be observed and the primary amines, -NH_2 on the organic linker can be clearly seen at 3394 and 3480 cm^{-1}, referring to symmetric and asymmetric vibrations of NH_2 groups, while the bridging OH group can be observed at 3675 cm^{-1} [21].

[Insert Fig.1]

From the spectrum of amino-Zr-MOF after heating at 300 °C, it was found that the intensities of peaks at 1564, 1497, 1424 and 1384 cm^{-1} were reduced. Also, the width of the band 1479-1785 cm^{-1} was reduced, indication of collapse of the structure. This can be confirmed by TGA profiles of amino-Zr-MOF (Fig. 2), which showed a broad weight loss process at 350 °C on amino-Zr-MOF treated at 300 °C, due to breakup of the interconnection between the functional groups and oxygen of metal centre inside the pores. Meanwhile, the weight loss profile of amino-Zr-MOF treated at 200 °C showed two weight loss processes at 350 – 550 °C, suggesting the presence of the interconnection binding. By breaking this interconnection, the whole structure of Zr-MOF was collapsed and the most pores were blocked. In a previous report, such a weight loss was not found [14], due to a different activation process.

[Insert Fig.2]

XRD patterns of amino-Zr-MOFs are illustrated in Fig.3. The profiles of the as-synthesised amino-Zr-MOF and amino-Zr-MOF activated at 200 °C were similar and show a similar pattern of UiO-66 as reported in the previous investigation [13]. However, the sample XRD after activation at 300 °C was totally different. The XRD profile presented a broad peak at 2θ = 7.5°, suggesting amorphous structure due to the collapse of crystalline structure. This further confirmed the FTIR and TGA results.

[Insert Fig.3]

The nitrogen isotherms and pore size distributions of amino-Zr-MOFs are presented in Fig.4. It can be seen that amino-Zr-MOF activated at 200 °C presented a highly developed microporous structure with much higher N_2 adsorption than the sample after heating treatment at 300 °C. The pore size distribution of amino-Zr-MOF activated at 200 °C showed two peaks centred at 1.5 and 3.3 nm, respectively. However, amino-Zr-MOF activated at 300 °C showed a shift of pore size to larger pore range. The two peaks were changed to 2.4 and 4.4 nm, respectively.

[Insert Fig.4]

The BET surface area of amino-Zr-MOF activated at 200 °C was 1220 m^2/g while the Langmuir surface area was 1395 m^2/g. The average pore radius was 0.99 nm and the total pore volume was 0.611 cm^3/g. The surface area of this sample is similar to the result reported by Zlotea et al. [24]. However, the BET surface area of the sample activated at 300 °C was significant reduced to 180 m^2/g, which reflects the destruction of porous structure. A comparison of amino-Zr-MOF with other MOFs shows that amino-Zr-MOF still has high porosity (Table 1). These above results suggested that activation of as-synthesised amino-Zr-MOF could be only done below 300 °C. Above 300 °C, the crystalline structure of amino-Zr-MOF could be destroyed to produce amorphous phase.

Table 1. BET surface area of different amino functionalized metal organic frameworks

Sample	$S_{BET}(m^2/g)$	Reference
MIL-125(Ti)	1130	[24]
UiO-66(Zr)-NH$_2$	1206(1280)	[24]
IRMOF-3 DEF	3683	[25]
Amino-MIL-53(Al)	675	[25]
Amino-MIL-101(Al)	2100	[26]
Amino-Zr-MOF	1220	This work

Fig. 5 shows SEM photo of amino-Zr-MOF. As seen, amino-Zr-MOF presented as symmetrical crystals with triangular base-pyramid shape and the particle size was about 200 nm.

[Insert Fig.5]

3.2 Adsorption study

Fig. 6 displays CO_2 adsorption isotherms on amino-Zr-MOF at 0 and 23 °C. Amino-Zr-MOF showed good adsorption of CO_2 and the capacity depended on temperature. At 1 atm, 0 °C, CO_2 adsorption could reach 4.46 mmol/g, which is higher than that on Zr-MOF (3.52 mmol/g)[17]. This could be attributed to the presence of basic amino groups in porous structure. In addition, the adsorption of CO_2 at 23 °C was reduced and the capacity was determined as 2.85 mmol/g. Heat of adsorption was calculated using the Clausius-Clapeyron equation ($dp/p=\Delta H \, dT/RT^2$) and an average value from different CO_2 coverage on amino-Zr-MOF was obtained as 29.4 kJ/mol. Table 2 presents the heat of CO_2 adsorption on various amino-functionalised MOFs. The value of amino-Zr-MOF is reasonable in comparison with other amino-functionalised MOFs [27]. The relatively higher values of the heat of CO_2 adsorption is due to amino groups which could create an electric field inside the pores against more polarisable adsorbates [28]. In addition, the free primary amine present in amino-Zr-MOF would form a carbamate with the CO_2, resulting in high energy.

[Insert Fig.6]

Table 2. Heat of CO_2 adsorption on different amino-functionalised MOFs.

Sample	CO_2 Heat of adsorption(kJ/mol)	Reference
IRMOF-3 DEF	20	[25]
Amino-MIL-53(Al)	38	[25]
Amino-MIL-101(Al)	28	[26]
Zr-MOF	28	[29]
Amino-Zr-MOF	29.3	This work

Amino-Zr-MOF was also tested at high pressure up to 980 kPa at 0 °C for CO_2 and CH_4 adsorption and the adsorption isotherms are presented in Fig.7. As seen, CH_4 and CO_2 adsorption increased with increasing pressure and CO_2 adsorption was higher than CH_4. The adsorption values were 9.04 and 3.73 mmol/g for CO_2 and CH_4, respectively at 980 kPa. The ideal selectivity of CO_2 to CH_4 was obtained based on ratio of the equilibrium adsorption at varying pressures and is shown in Fig.7. It is seen that the ideal selectivity of CO_2/CH_4 on

amino-Zr-MOF decreased with increasing pressure and it ranged from 4.5 to 2.35 over the range of pressure between 0.3 and 9 atm, 0 °C.

[Insert Fig.7]

From adsorption column tests shown in Fig. 8, it was proved that this material had a good capacity to adsorb carbon dioxide in real conditions. The breakthrough time changed with the variation of CO_2 concentration. It was 40, 31, 20 min at 10%, 15% and 20% CO_2, respectively, in CO_2-N_2 gas mixture passing through the adsorption column. From the breakthrough curve it was shown that the slope of the curve increased sharply and with increase in CO_2 concentration, suggesting no diffusion limitations in the material during the adsorption. Also, the high slope of these curves may refer to the possibility of adsorbent regeneration directly after reaching saturation, which can be a good indication toward reducing the cost of gas regeneration [30]. By the integration of the curves, total adsorbed amount of CO_2 within the column during the breakthrough time could be calculated as around 4.55, 5.26 and 4.37 mmol/g at 10%, 15% and 20%CO_2, respectively.

The adsorption capacities obtained at dynamic tests at 10% and 20%CO_2 are in a good agreement with the value obtained from the static volumetric adsorption (4.46 mmol/g) whereas the value is higher at 15% CO_2. The high CO_2 adsorption obtained at 15%CO_2 was probably attributed to the dynamic exchange equilibrium of CO_2 with N_2. Before CO_2 adsorption, Zr-MOF column was saturated with N_2. At lower CO_2 concentration, the exchange of N_2 by CO_2 may take longer time, resulting in a fast effluent of CO_2 and overestimation of CO_2 adsorption at 15%CO_2.

[Insert Fig.8]

4. Conclusion

An amino-Zr-MOF was synthesised with methanol activation and heating treatment at temperature below 300 ºC. It was found that activating temperature played an important role for the porous structure of amino-Zr-MOF. The amino-Zr-MOF exhibited higher thermal stability and higher CO_2 adsorption than CH_4. The CO_2/CH_4 ideal selectivity decreased with increasing pressure. Static isothermal measurement and column tests showed that CO_2 adsorption at 1 atm is around 5 mmol/g. At higher pressure of 10 atm, CO_2 adsorption could reach 9 mmol/g.

References

[1] A.M. Wolsky, E.J. Daniels, and B.J. Jody, *CO₂ capture from the flue gas of conventional fossil-fuel-fired power plants*, Environ. Progress, 13 (1994), pp. 214-219.

[2] G. Ferey, C. M. Draznieks, C. Serre, and F. Millange, *Crystallized frameworks with giant pores: are there limits to the possible?* Acc. Chem. Res., 38 (2005), pp. 217-225.

[3] U. Mueller, M. Schubert, F. Teich, H. Puetter, K. Schierle-Arndt, and J. Pastre, Metal–organic frameworks-prospective industrial applications, J. Mater. Chem, 16 (2006), pp.626-636.

[4] M. Gallo, and D. Glossman-Mitnik, *Fuel gas storage and separations by metal-organic frameworks: simulated adsorption isotherms for H_2 and CH_4 and their equimolar mixture*, J. Phys. Chem. C, 113 (2009), pp. 6634–6642.

[5] P. Horcajada, C. Serre, G. Maurin, N. A. Ramsahye, F. Balas, M. Vallet-Regí, M. Sebban, F. Taulelle, and G. Férey, *Flexible porous metal-organic frameworks for a controlled drug delivery*, J. Am. Chem. Soc., 130 (2008), pp. 6774–6780.

[6] Wu C.D., Hu A. Zhang L., and Lin W., *A homochiral porous metal-organic framework for highly enantioselective heterogeneous asymmetric catalysis*, J. Am. Chem. Soc., 127 (2005), pp. 8940-8941.

[7] Chen B., Yang Y., Zapata F., Lin G., Qian G., and Lobkovsky E. B., *Luminescent open metal sites within a metal-organic framework for sensing small molecules*, Adv. Mater., 19 (2007), pp. 1693–1696.

[8] J. L. C. Rowsell, E.C. Spencer, J. Eckert, J.A.K. Howard, and O. M. Yaghi, *Gas adsorption sites in a large-pore metal-organic framework*, Science, 309 (2005), pp. 1350-1354.

[9] R.Q. Snurr, J. T. Hupp, and S. T. Nguyen, *Prospects for nanoporous metal-organic materials in advanced separations processes*, AIChE J., 50 (2004), pp. 1090-1095.

[10] S. L. James, *Metal organic frameworks*, Chem. Soc. Rev. 32 (2003), pp. 276-288.

[11] O. M. Yaghi, M. O'Keeffe, N. W. Ockwig, H. K. Chae, M. Eddaoudi, and J. Kim, *Reticular synthesis and the design of new materials*, Nature 423 (2003), pp. 705-714.

[12] J. Nawrocki, M.P. Rigney, A. McCormik, P. W. Carr, *Chemistry of zirconia and its use in chromotography*, J. Chromato A. 657 (1993), pp. 229-282.

[13] J. H. Cavka, S. Jakobsen, U.Olsbye, N. Guillou, C. Lamberti, S. Bordiga, and K. P. Lillerud, *A new zirconium inorganic building brick forming metal organic frameworks with exceptional stability*, J. Am. Chem. Soc., 130 (2008), pp. 13850–13851.

[14] Kandiah M., Nilsen M.H., Usseglio S. Jakobsen S., Olsbye U., Tilset M., Larabi C. Quadrelli E. A., Bonino F. , and Lilerud K. P. *Synthesis and stability of tagged UiO-66 Zr-MOF*, Chem. Mater. 22 (2010), pp. 6632-6640.

[15] C.G. Silva, I. Luz, F. X. L. Xamena, A. Corma, and H. Garcia, *Water stable Zr-benzendicarboxylate metal-organic frameworks as photocatalysts for hydrogen generation,* Chem. Eur. J. 16 (2010), pp. 11133-11138.

[16] F. Vermmortele, R. Ameloot, A. Vimont, C. Serre, and D. D. Vos, *An amino-modified Zr-terephthalate metal-organic framework as an acid–base catalyst for cross-aldol condensation*, Chem. Commun, 47 (2011), pp. 1521-1523.

[17] H. R. Abid, G. H. Pham, H. M. Ang, M. O. Tade, S. B. Wang, *Adsorption of CH_4 and CO_2 on Zr-metal-organic-frameworks*, J. Colloid Interface Sci., 366 (2012), pp. 120-124.

[18] T. Loiseaau, C. Serre, C. Huguenard, G. Fink, F. Taulelle, M. Henry, T. Bataille, and G. Ferey, *A rationale for the large breathing of the porous aluminum terephthalate(MIL-53) upon hydration*, Chem. Eur. J. 10 (2004), pp. 1373 -1382.

[19] E. Biemmi, T. Bein, N. Stock, *Synthesis and characteristics of a new metal organic frameworks structure with a 2D porous system;$(H_2Net_2)_2\{Zn_3(BDC)_4\}.3DEF,$* Solid State Sci., 8 (2006), pp.363-370.

[20] S. Bauer, C. Serre, T. Devic, P. Horcajada, J. Marrot, G. Frey, and N. Stock, *High-throughput assisted rationalization of the formation of metal organic frameworks in the iron(III) aminoterephthalate solvothermal system,* Inorg. Chem., 47 (2008), pp 7568–7576.

[21] A. L. Grzesiak, F.J. Uribe, N. W. Ockwig, O. M. Yaghi, and A.J. Matzger, P*olymer-induced heteronucleation for the discovery of new extended solids,* Angew. Chem. Int. Ed. 45 (2006), pp. 2553 –2556.

[22] E. Stavitski, E.A. Pidko, S. Couck, T. Remy, E. J. M. Hensen, B. M. Weckhuysen, J. Denayer, J. Gascon, and F. Kapteijn, *Complexity behind CO_2 capture on NH_2-MIL-53(Al)*, Langmuir, 27 (2011), pp. 3970–3976.

[23] T. Ahnfeldt, D. Gunzelmann, T. Loiseau, D. Hirsemann, J. Senker, G. Ferey, and N. Stock, *Synthesis and modification of a functionalized 3d open-framework structure with MIL-53 topology*, Inorg. Chem., 48 (2009), pp. 3057-3067.

[24] C. Zlotea, D. Phanon, M. Mazaj, D. Heurtaux, V. Guillerm, C. Serre, P. Horcajada, T. Devic, E. Magnier, F. Cuevas, G. Férey, P. L. Llewellyn, and M. Latroche, *Effect of*

NH$_2$ and CF$_3$ functionalization on the hydrogen sorption properties of MOFs, Dalton Trans., 40 (2011), pp.4879-4881.

[25] J. Gascon , U. Aktay, M. D. Hernandez-Alonso, G. P.M. van Klink, and F. Kapteijn, *Amino-based metal-organic frameworks as stable, highly active basic catalysts.* J. Catal. 261 (2009), pp. 75-87.

[26] P. Serra-Crespo, E.V. Ramos-Fernandez, J. Gascon, and F. Kapteijn, S*ynthesis and characterization of an amino functionalized mil-101(al): separation and catalytic properties*" Chem. Mater., 23 (2011), pp. 2565–2572.

[27] S. Couck, F. M. Denayer, G. V. Baron, J. Gascon, F. Kapteijn, *An amino-functionalized MIL-53 metal organic framework with large separation power for CO$_2$ and CH$_4$,* J. Am. Chem. Soc., 131 (2009), pp. 6326-6327.

[28] D. Farrusseng, C. Daniel, C. Gaudill, U. Ravon, Y. Schuurman, C. Mirodatos, D. Dubbeldam, H. Frost, and R. Q. Snurr, *Heats of adsorption for seven gases in three metal-organic frameworks: systematic comparison of experiment and simulation,* Langmuir, 25 (2009), pp. 7383–7388.

[29] H. R. Abid, H. Y. Tian, H. M. Ang, M. O. Tade, C. E. Buckley, S. B. Wang, *Nanosize Zr-metal organic framework (UiO-66) for hydrogen and carbon dioxide storage,* Chem. Eng. J., 185-186 (2012), pp.328-336.

[30] A. Douglas and T. Costas, *Separation of CO$_2$ from flue gas: A review*, Sep. Sci. Technol., 40 (2005), pp. 321-348.
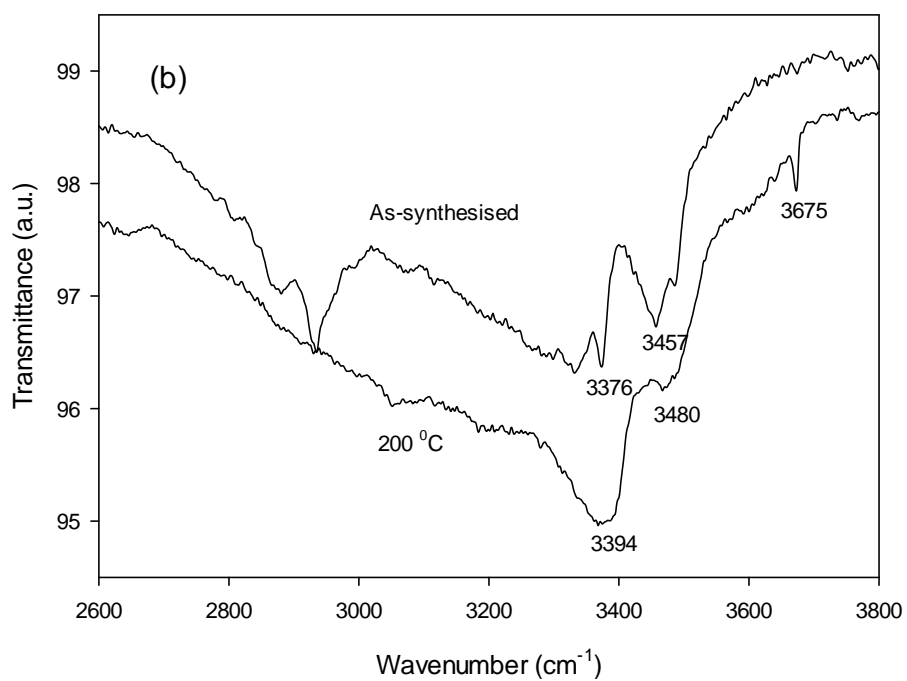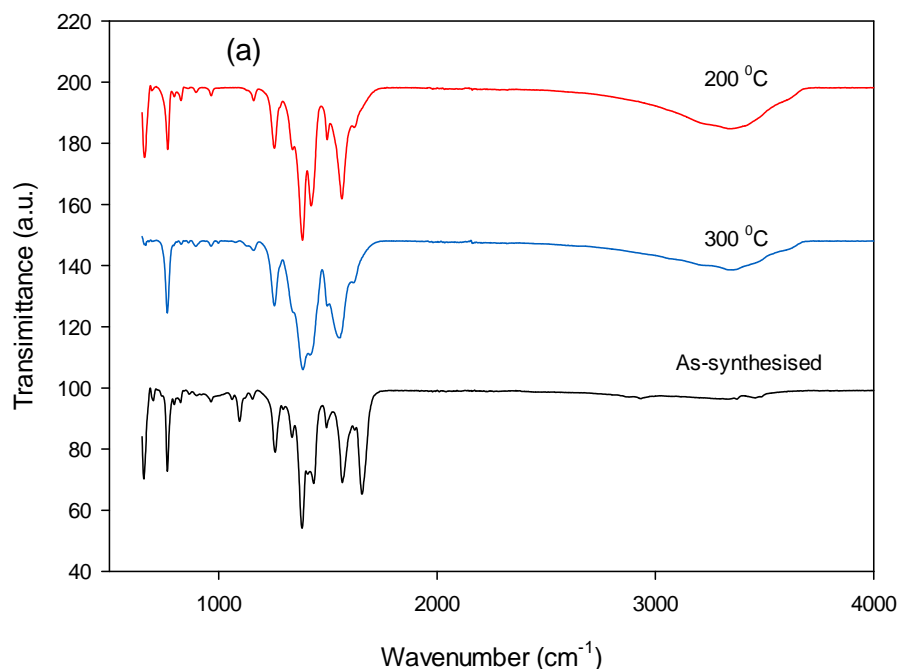
List of Figures

Fig.1 FTIR spectra of amino-Zr-MOFs (a), magnification of the band at 2600-3800 cm^{-1} of as-synthesised amino-Zr-MOF (b).
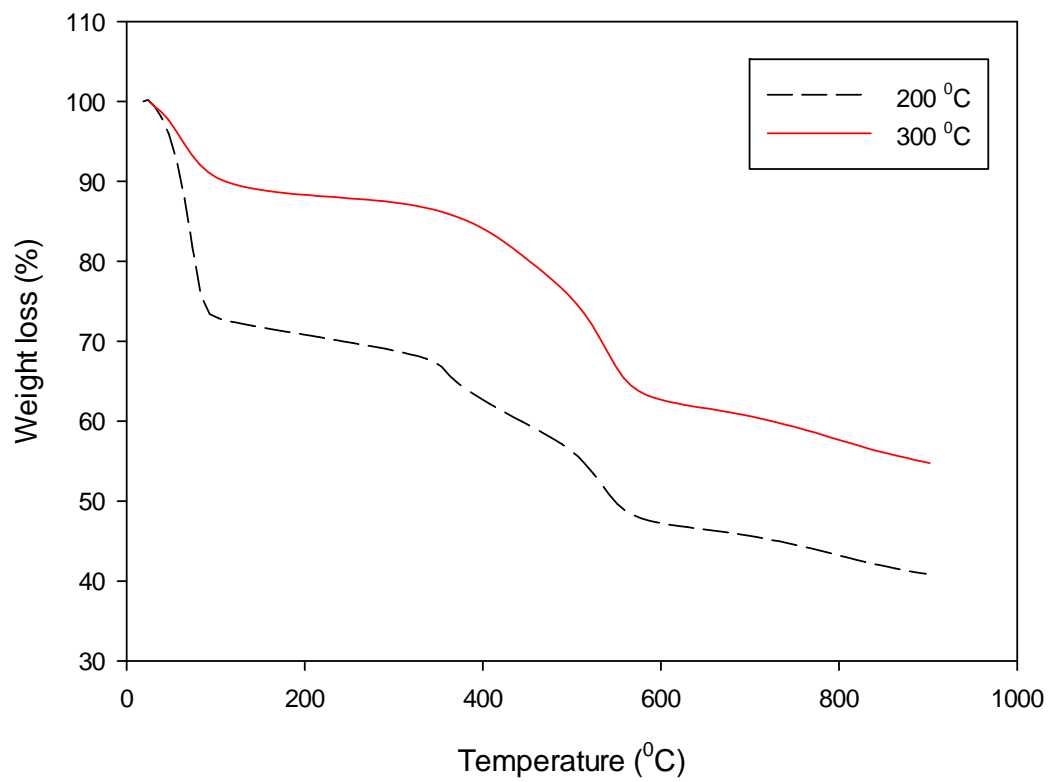
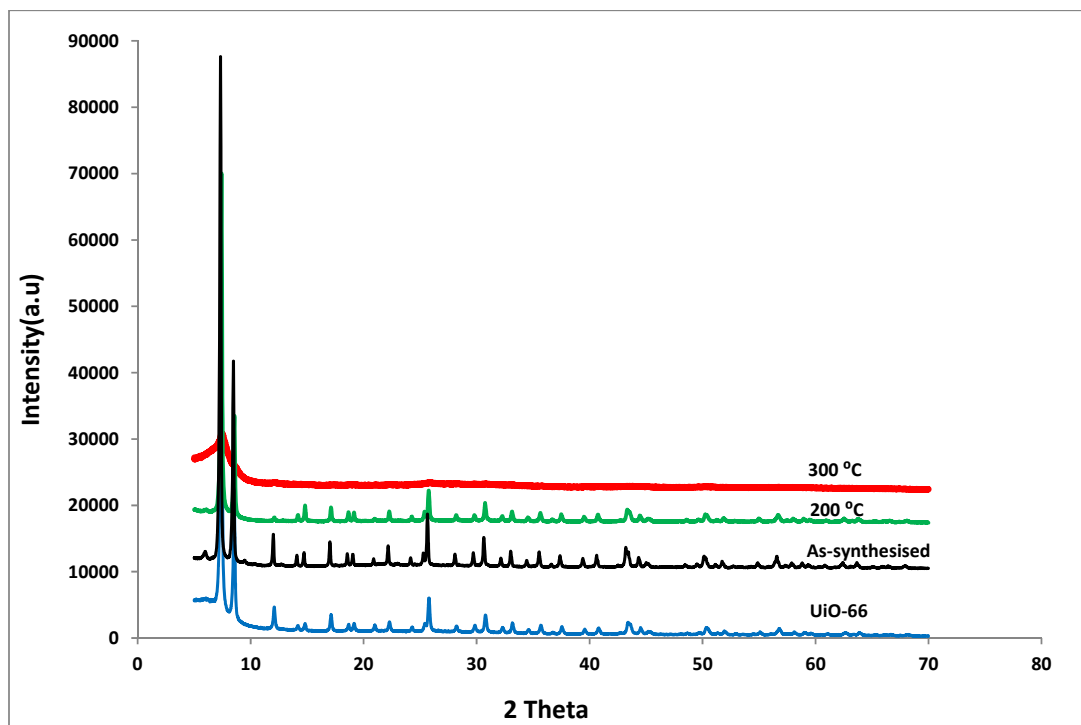Fig. 2 TGA profiles of amino-Zr-MOF activated by methano and heating under 200 and 300 °C.

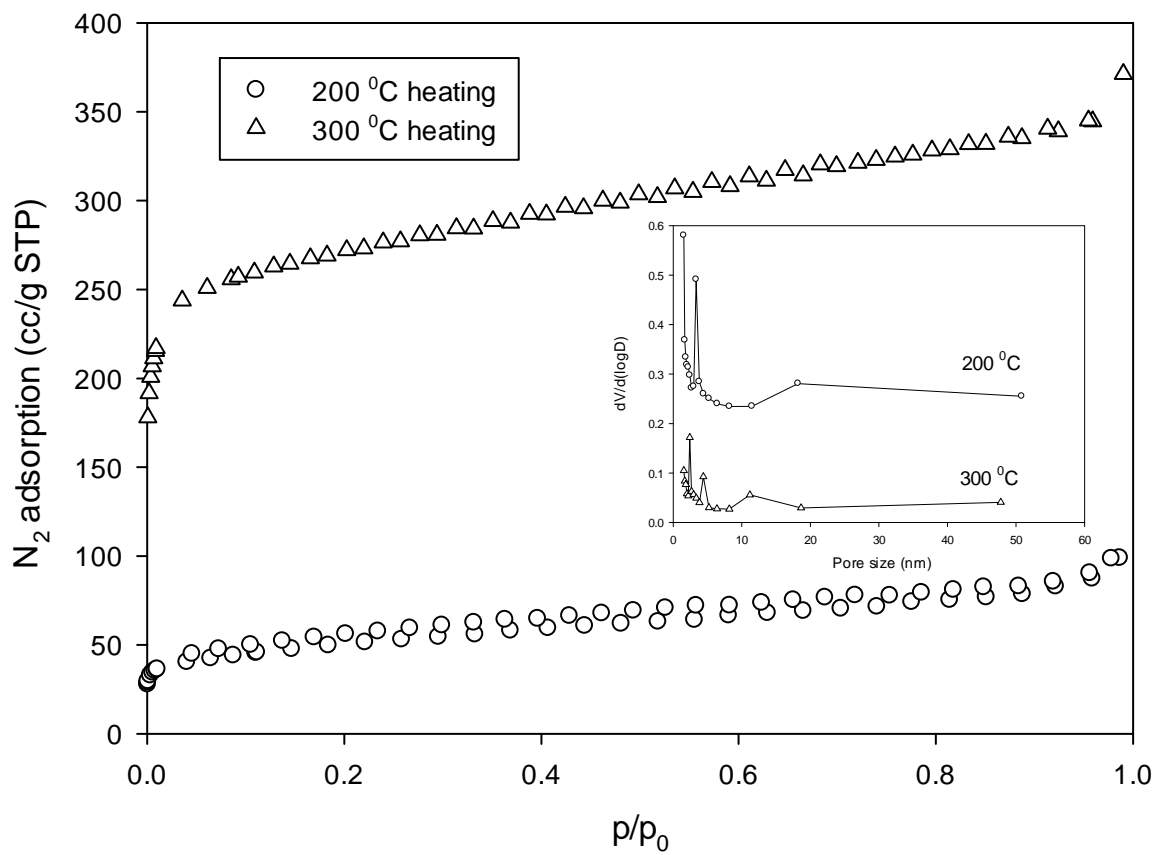Fig.3 XRD patterns of amino-Zr-MOFs activated at different temperatures.

Fig.4 N_2 adsorption isotherm and pore size distributions of amino-Zr-MOFs activated at different temperatures.
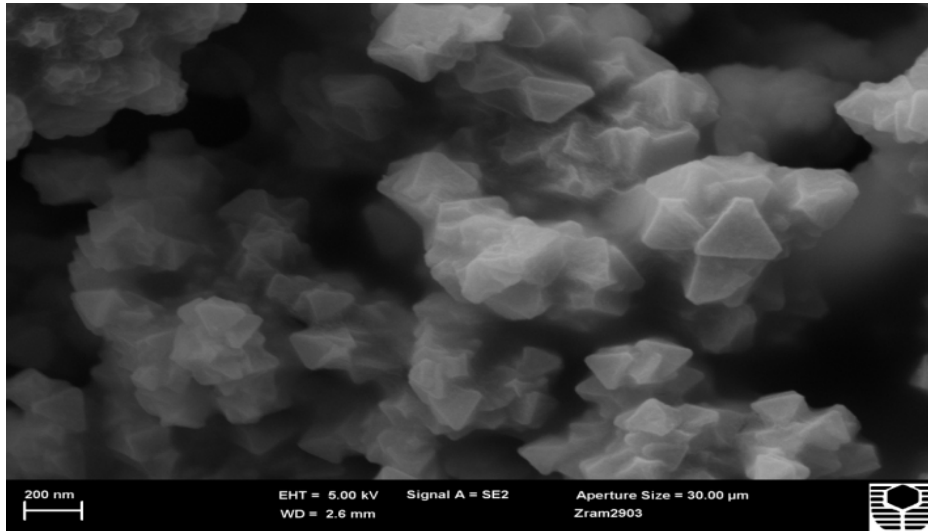
Fig.5 SEM image of activated amino-Zr-MOF.

Fig.6 CO_2 adsorption on amino-Zr-MOF at different temperatures.

Fig.7 CO_2 and CH_4 adsorption on amino-Zr-MOF and ideal selectivity.

Fig.8 Breakthrough curves of CO_2 adsorption at different CO_2 concentrations.

Fig.1 FTIR spectra of amino-Zr-MOFs (a), magnification of the band at 2600-3800 cm^{-1} of as-synthesised amino-Zr-MOF (b).

Fig. 2 TGA profiles of amino-Zr-MOF activated by methano and heating under 200 and 300 °C.

Fig.3 XRD patterns of amino-Zr-MOFs activated at different temperatures.

Fig.4 N_2 adsorption isotherm and pore size distributions of amino-Zr-MOFs activated at different temperatures.
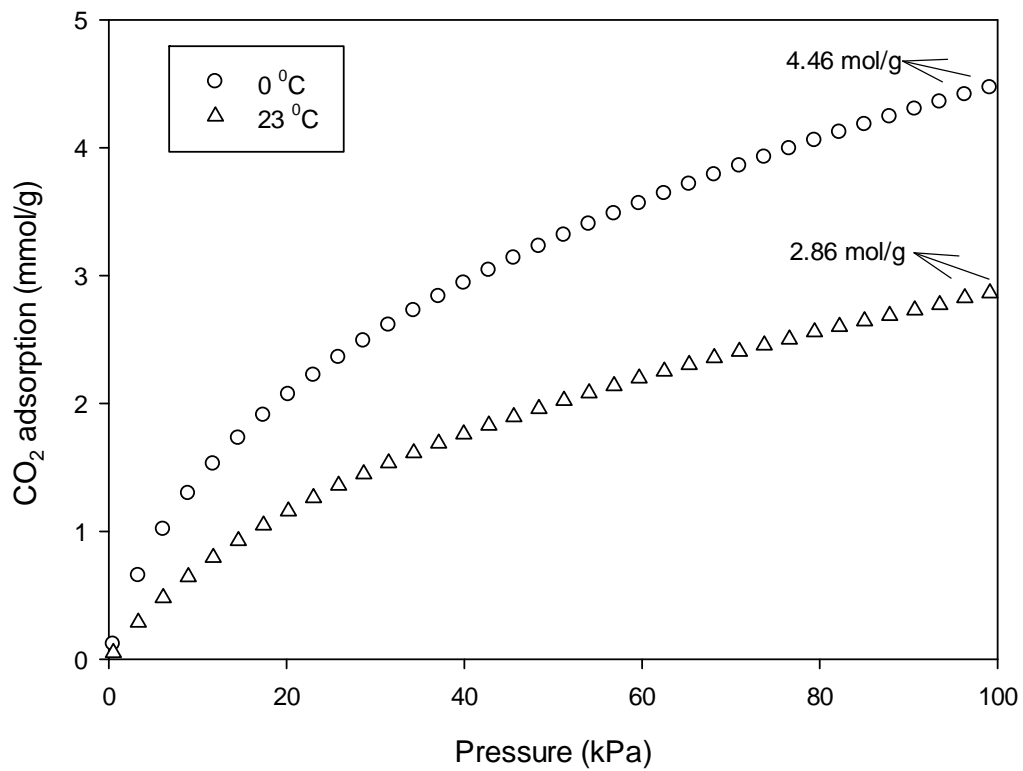
Fig.5 SEM image of activated amino-Zr-MOF.

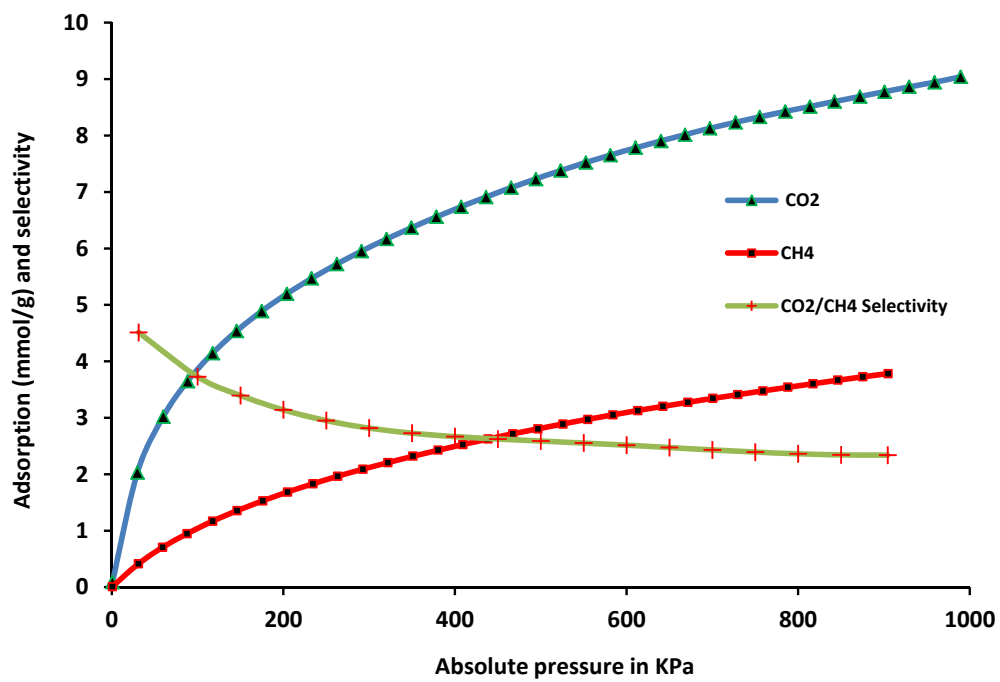Fig.6 CO_2 adsorption on amino-Zr-MOF at different temperatures.

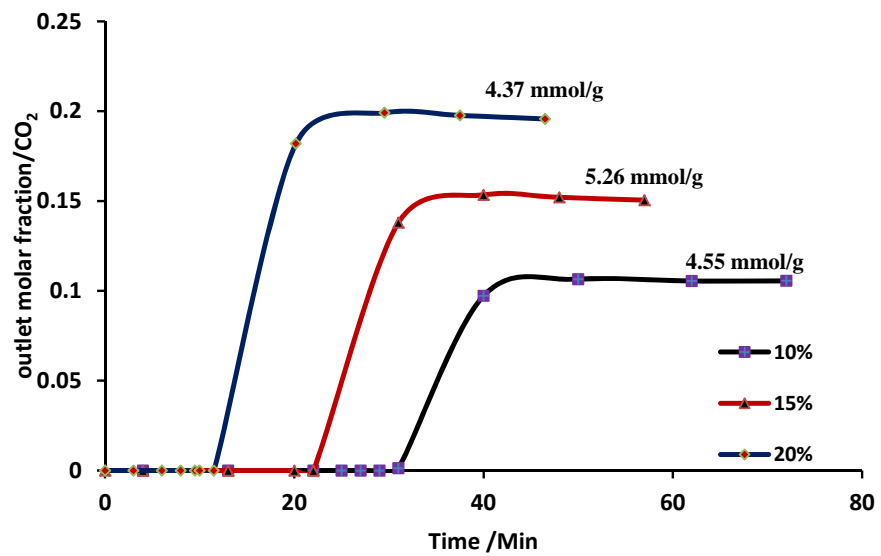Fig.7 CO_2 and CH_4 adsorption on amino-Zr-MOF and ideal selectivity.

Fig.8 Breakthrough curves of CO_2 adsorption at different CO_2 concentrations.